

Article

# Fast Electrical Characterizations of High-Energy Second Life Lithium-Ion Batteries for Embedded and Stationary Applications

**Honorat Quinard** <sup>1,2,†</sup>, **Eduardo Redondo-Iglesias** <sup>1,\*</sup>, **Serge Pelissier** <sup>1</sup> and **Pascal Venet** <sup>2</sup><sup>1</sup> Univ Lyon, IFSTTAR-AME-Eco7, 69500 Bron, France; honoratquinard@gmail.com (H.Q.); serge.pelissier@ifsttar.fr (S.P.)<sup>2</sup> Univ Lyon, Université Claude Bernard Lyon 1, Ecole Centrale de Lyon, INSA Lyon, CNRS, Ampère, F-69007 Lyon, France; pascal.venet@univ-lyon1.fr

\* Correspondence: eduardo.redondo@ifsttar.fr; Tel.: +33-472-14-24-76

† Former Ph.D. Student Funded by Carwatt at IFSTTAR and Ampere laboratory, 69675 Bron Cedex, France.

Received: 31 January 2019; Accepted: 12 March 2019; Published: 14 March 2019



**Abstract:** This paper focuses on the fast characterization of automotive second life lithium-ion batteries that have been recently re-used in many projects to create battery storages for stationary applications and sporadically for embedded applications. Specific criteria dedicated to the second life are first discussed. After a short review of the available state of health indicators and their associated determination techniques, some electrical characterization tests are explored through an experimental campaign. This offline identification aims to estimate the remaining ability of the battery to store energy. Twenty-four modules from six different commercial electric vehicles are analyzed. Well-known methodologies like incremental capacity analysis (ICA) and constant voltage phase analysis during CC-CV charge highlight the difficulty—and sometimes the impossibility—to apply traditional tools on a battery pack or on individual modules, in the context of real second life applications. Indeed, the diversity of the available second life batteries induces a combination of aging mechanisms that leads to a complete heterogeneity from a cell to another. Moreover, due to the unknown first life of the battery, typical state of health determination methodologies are difficult to use. A new generic technique based on a partial coulometric counter is proposed and compared to other techniques. In the present case study, the partial coulometric counter allows a fast determination of the capacity aging. In conclusion, future improvements and working tracks are addressed.

**Keywords:** second life battery; lithium-ion; electrical characterization; state-of-health (SOH); partial coulometric counter

## 1. Introduction

### 1.1. Deployment of Electric Vehicles and Arrival of Second Life Batteries

The democratization of the electric vehicle in our modern society is nowadays an undeniable fact. Since 2010, the share of electric car holder scaled up significantly, reaching 3 million units in 2017 [1] and the Paris Declaration [2] in 2015 encouraged this phenomenon. According to the International Energy Agency [1] the global electric car stock for 2030 should raise up to 56 million units.

However, the decarbonisation of our transportation system has an insidious environmental drawback. That global trend is going to generate millions of used batteries and recycling processes are not ready to handle such quantities especially with heterogeneous chemistries. Before the question of recycling, the idea of a possible circular economy market around the second life of batteries is

an upcoming question and many pioneer projects are now using automotive lithium-ion second-life batteries to store energy.

For example, research programs are using second life lithium-ion batteries like at University of California San Diego with a 160 kWh storage built from BMW batteries [3]. Nissan equipped its regional office in France with 100 vehicle-to-grid bi-directional chargers supplied by Enel, with an energy storage system combining 64 Nissan Leaf packs installed by Eaton [4]. EDF (Électricité de France), Forsee Power, Mitsubishi Motors Corporation, Mitsubishi Corporation and PSA Peugeot Citroën announced to jointly study the possibility of the energy storage business in Europe utilizing lithium-ion batteries from electric vehicles and launched a demonstration project in September 2015 in France at Forsee Power's new Headquarter near Paris [5]. Even domestic applications are considered like the power wall from Tesla [6] and the xStorage by Eaton [7]. More recently, start-ups like Carwatt [8] are trying to use second life lithium-ion batteries in different electric vehicle conversion projects.

### 1.2. Heterogeneity of State of Health in Second Life Batteries

An example of a first life lithium-ion battery pack, sold by the car manufacturer Renault, is illustrated in Figure 1. After few years of service, modules become heterogeneous and according to the origin and the life of the battery pack the phenomenon can increase. In order to build a brand new homogeneous second life battery pack, modules have to be dismantled and selected according to their SOH.

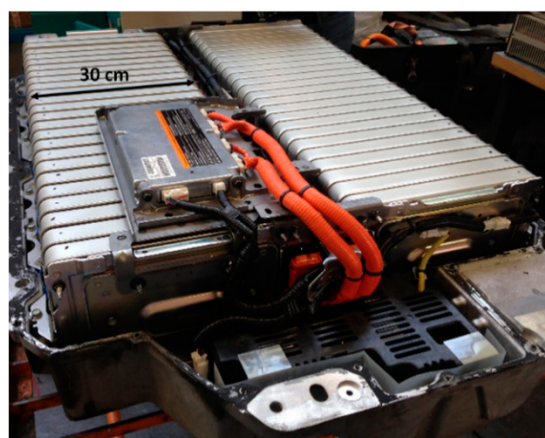


**Figure 1.** Renault KANGOO battery pack with AESC 65 Ah modules stored in CARWATT's workshop [8].

From stationary to embedded applications, scientific problems are addressed to the research community especially regarding the determination of the battery state of health (SOH). This identification has to be fast, cheap and robust in order to provide a competitive advantage compared to another substitute product like fresh battery, other technologies and to develop, by consequence, a real second life battery industry.

The main goal of a SOH measurement is to point out systemic limitations that could be brought by second life batteries to the future repurposed energy storage system (ESS).

Indeed, a lithium-ion battery degrades mainly by capacity and power fading but whether in the industry or in the research community, no clear consensus about a single definition of the state of health has been found. Most of the time, capacity and impedance are used to define the SOH. Frequently, car manufacturers consider that a loss of 20% of the initial capacity or a 200% impedance increase are good signatures to evaluate the end of the first life.

The SOH related to the capacity is generally defined by Equation (1):

$$SOH(Q)[\%] = 100 \frac{Q_m}{Q_{nominal}} \quad (1)$$

where  $Q_m$  is the measured capacity during the test and  $Q_{nominal}$  the nominal capacity of a fresh cell under the same experimental conditions.

The SOH related to the impedance is generally defined by Equation (2):

$$SOH(Z)[\%] = 100 \left( 2 - \frac{Z_m}{Z_{nominal}} \right) \quad (2)$$

where  $Z_m$  is the measured impedance during the test and  $Z_{nominal}$  the nominal impedance of a fresh cell under the same experimental conditions.

Most of the time, second life battery modules are not produced anymore and electrochemical cell features are not available. Then, a classification based on a fresh reference is not possible. A way to solve this issue is to compare one module to each other with an average value provided by a specific methodology as presented in this paper. The characterization process has to be realized as fast as possible especially for economic reasons.

### 1.3. Need of Specific Methods for Determination of SOH

The basic method mainly used to measure the capacity is to fully charge or discharge a battery. This protocol is very time consuming since modules have to be tested one by one. Moreover, in practical case, second-life modules could be supplied by car manufacturers at various SOC (from 35% to 75%) adding preparation test time. These last observations lead to the impossibility to apply directly the aforementioned protocol.

New techniques have been explored by researchers through years. Berecibar et al. [9] reviewed the existing SOH estimation methods and classified in specific groups the different approaches. Adaptive methods like Kalman filter [10,11], neural networks [12,13], and many others are very accurate but computational resources and development are also complex [14]. On the opposite, empirical techniques mainly based on capacity and impedance measurements are simple and very effective methods but they are highly dependent on the operating conditions [15,16]. A third group using differential analysis can detect the degradation mechanisms with the advantages of both adaptive and empirical techniques, namely accuracy and low computational efforts [17].

Some approaches have already been tested and validated to evaluate the impedance of the battery within a short amount of time. Pilatowic et al. [18] define and describe various impedance estimation methodologies. Batteries' internal impedance is nonlinear and demonstrates different ohmic, capacitive and inductive behaviours according to the frequency. Then, it appears that the major concern is not really related to the measurement protocol itself but mostly how to interpret and how to give the right figure of merit to the internal impedance value.

On the opposite, there is an apparent lack of methodologies when it comes to a quick capacity fading estimation. Therefore, the present article is going to focus on fast offline approaches based on experimental measurements that can identify the capacity loss of a second life lithium-ion battery.

Incremental Capacity Analysis (ICA) is a well-known technique and this mathematical tool initially used by electrochemists, is gaining more and more credit in the battery community. Through peak area analysis (Riviere et al. [19]) or peak position analysis (Ans  an et al. [20]) a deep understanding of the aging mechanisms can be achieved. It requires static charge/discharge at very low C-rate (C/20) which generate very long periods of test. This initial drawback has been solved and different researches proved that higher C-rate (up to C/2) and truncated profiles (Li et al. [21]) could provide sufficient information about the capacity fading.

Eddahech et al. [22] analysed the charge current profile occurring throughout the constant voltage step. Indeed, the current time constant which in fact, represents the kinetic of the lithium-ions intercalation process into the negative electrode can give an accurate representation of the capacity fading phenomenon. Yang et al. [23] extended this methodology and proposed to study a partial CV charge reducing by consequence, the estimation time.

Results of the two previous techniques, standing on real aged second life lithium-ion batteries experimental campaign (realized in IFSTTAR and Ampere laboratories), demonstrate the impossibility to apply actual protocols with a good accuracy or within a short amount of time on a unique module. Consequently, the need of a specific approach to characterize an individual second life lithium-ion battery is corroborated and a new generic technique based on a partial coulometric counter is proposed.

## 2. Experimental Setup and Methods

### 2.1. Data Acquisition System

All the experiments were performed using a battery module tester Bitrode FTV2 (2 channels/0–250 A) with a resolution of 1 mV/10 mA and an electrochemical impedance spectrometer Biologic VSP+VMP (3 channels/0–20 A) with a resolution of 1 mV/20 mA test bench. In this experiment, data acquisition systems have a maximum sampling frequency of 10 Hz. The temperature is set and controlled at 25 °C into a climatic chamber.

### 2.2. Cell Specifications

The experimental part was realized on aged high energy modules made from pouch cells. These batteries sold by the manufacturer Automotive Energy Supply Corporation (AESC) are rated with a nominal capacity of 65 Ah.

Modules are extracted from six different aged battery packs which equipped the first generation of electric commercial vehicles, Renault KANGOO. Each pack is initially constituted by 48 modules in series as we can observe in Figure 1. The following study investigates the first four modules of each pack considering that this sample should give a good representativeness of the others.

A module is an association of two half modules in series. Each of them is composed of two unit cells in parallel. The module architecture is, therefore, 2P2S cells and voltage measurements are available for each half module as represented in Figure 2.

Half module 1 Half module 2

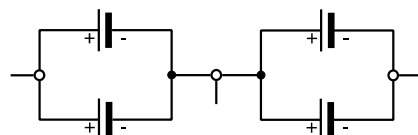


**Figure 2.** 2P2S unit cells.

By considering 24 samples represented in Figure 2, 48 half modules measurable separately are tested in coming paragraphs. Consequently, each tested sample is referenced as "Pack\_i\_m\_j\_halfmodule\_k" where "i" is pack number (1 to 6), "j" is module number (1–4) and "k" is the half-module number (1 or 2). Each of these tested samples, made of two unit cells in parallel is considered as a unique cell for the rest of the work. Considering the single cell characteristics given in Table 1, the initial value of the capacity of the tested samples was 65 Ah.

**Table 1.** Initial specifications of tested cells according to the manufacturer's datasheet.

AESC E5-M	
Cell type	Laminate Type
Positive electrode material	LMO with LNO
Negative electrode material	Graphite
Nominal capacity (at 0,3C)	32.5 Ah
Nominal voltage	3.75 V
Energy density	157 Wh/kg
Voltage limit range	2 to 4.2 V
Voltage operating range	2.5 to 4.15 V

The manufacturer AESC and the car manufacturer Renault recommendations give a voltage operating range for an optimal life expectancy of the cell which is from  $V_{min,op} = 2.5$  V to  $V_{max,op} = 4.15$  V. These values will frame the next experimental work.

### 2.3. Experimental Methods for SOH Estimation

Three different methods are presented in the following section and results will be compared in Section 3. The nominal capacity of each second life cell used as reference has been measured during a full CC discharge at 1C forerun by a wake up cycle.

#### 2.3.1. Constant Voltage Analysis during CC-CV Charge

One possible way to analyse the capacity loss of a battery is to study the CC-CV charge as in Figure 3. The standard and very common charging protocol can be divided into two distinct parts. First the constant current (CC) phase applies a constant current to the battery until the cut off voltage is reached then the battery remains at this voltage (CV) threshold in floating mode until the current reaches a minimal value determined most of the time by the battery management system, a typical value is C/20.

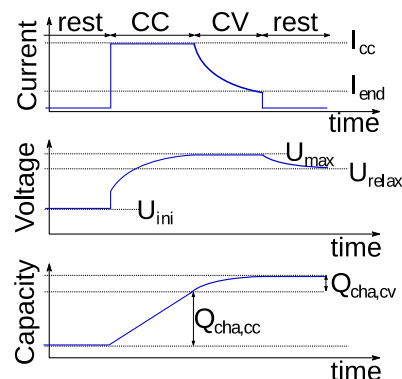


**Figure 3.** CC-CV charge cycle (Redondo-Iglesias et al. [24]).

The intercalation process of the lithium into the graphite negative electrode mainly takes place during the charge at constant current. For fresh cells only up to 5% of this chemical reaction occurs during the constant voltage step. Whereas for aged lithium-ion batteries an important part (from 32% to 45 %) of the available capacity is stored during the CV phase as shown in Figure 4.

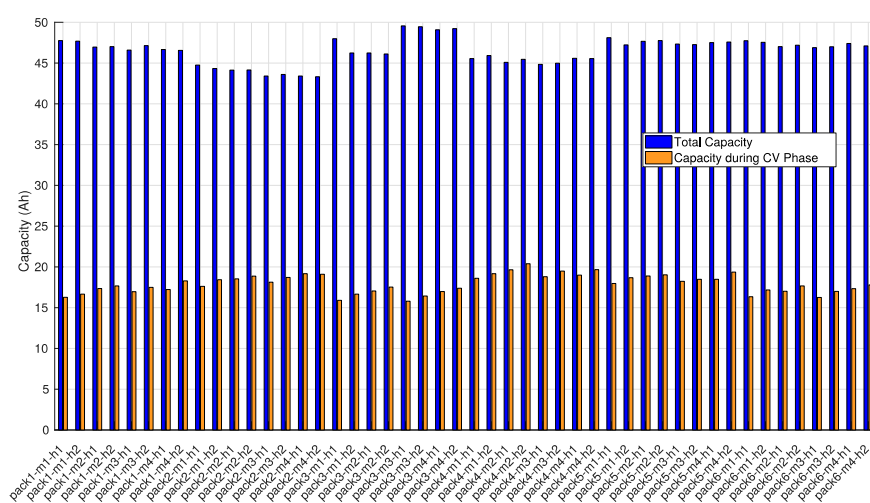


**Figure 4.** Capacity charged during the constant voltage phase and the full charge 1C for second life batteries.

This large amount of energy stored during the CV phase can be explained by the high value of the impedance. By consequence, the voltage upper limit during the CC phase is reached quicker than at its beginning of life increasing the role of the CV phase during the charge of the cell.

Eddahetch et al. [22] state that the kinetic of the potentiostatic mode (CV) at 1C is a pertinent indicator of the battery state of health and can indicate the capacity loss. In their approach, the measured CV current is fitted by a non-linear regression expressed by Equation (3):

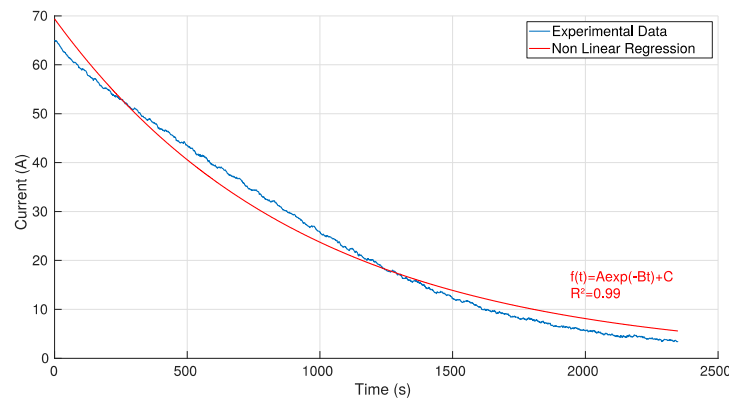
$$I(t) = Ae^{-Bt} + C \quad (3)$$

where  $B$  represents the kinetic of the battery during the CV charge and is used as an indicator of the state of health.

In Eddahetch et al. [22], the coefficient  $B$  has a good linear relation with the capacity loss of a battery for a capacity fading greater than 4% and up to 30%.

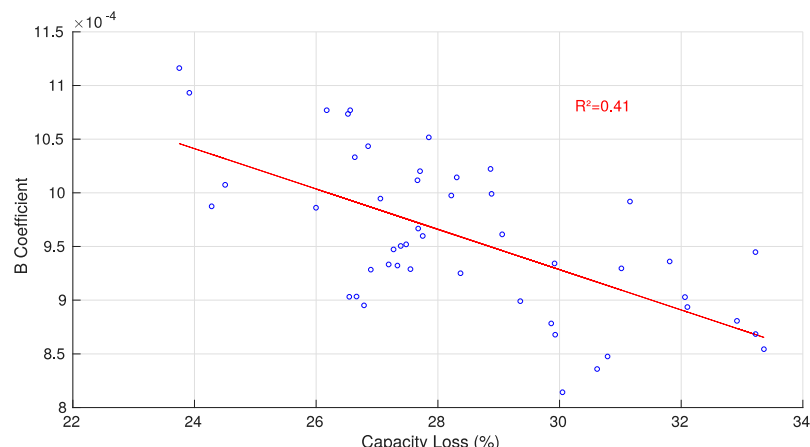
The described methodology previously applied by Eddahetch to follow the aging of one cell, was applied to our set of second life batteries composed of cells from different packs and at different SOH.

Figure 5 shows the correlation between the exponential regression and the experimental curve  $I(t)$  during the CV phase voltage. The quality of the fitting identified with the least square method is satisfactory ( $R^2 = 0.99$ ).



**Figure 5.** Comparison between measured and simulated current during CV step.

Experimental results from the aged battery test campaign are illustrated by Figure 6, where the quality of the correlation between the coefficient  $B$  and the capacity loss is identified using the least square method.



**Figure 6.** Evolution of the coefficient  $B$  according the capacity loss.

The  $R^2$  coefficient value ( $R^2 = 0.41$ ) of the correlation shows that the capacity fading cannot be correctly represented by any trend.

To sum up, this methodology seems difficult to use for a SOH determination in the context of the classification of second life lithium-ion batteries. At this point, the observation of the kinetic of the lithium insertion in the negative electrode is not sufficient anymore and advanced considerations will be presented in the final section of this paper.

### 2.3.2. Incremental Capacity Analysis

Incremental capacity analysis (ICA) is a mathematical tool based on the variation of the electric charge inside the battery considering the variation of the voltage across the electrodes. It can be described by Equation (4):

$$ICA \left[ \frac{Ah}{V} \right] = \frac{dQ}{dV} = \frac{\Delta Q}{\Delta V} \quad (4)$$

where  $Q$  is the capacity and  $V$  the voltage.

The method is based on the differentiation of the battery capacity over the battery voltage emphasizing the flat regions and the quick variations of the open circuit voltage curve (OCV). Each resulting peak (corresponding to the flat region of the OCV) and valley (corresponding to the evolution of the OCV) (Figure 7a,b) is unique and reflects electrochemical processes taking place into the battery. Then, peak area, position and shape can be analysed and interpreted. Characteristic features of the incremental capacity analysis are extremely correlated to the battery aging mechanisms and very accurate estimations of the capacity loss can be obtained (Dubarry et al. [25]).

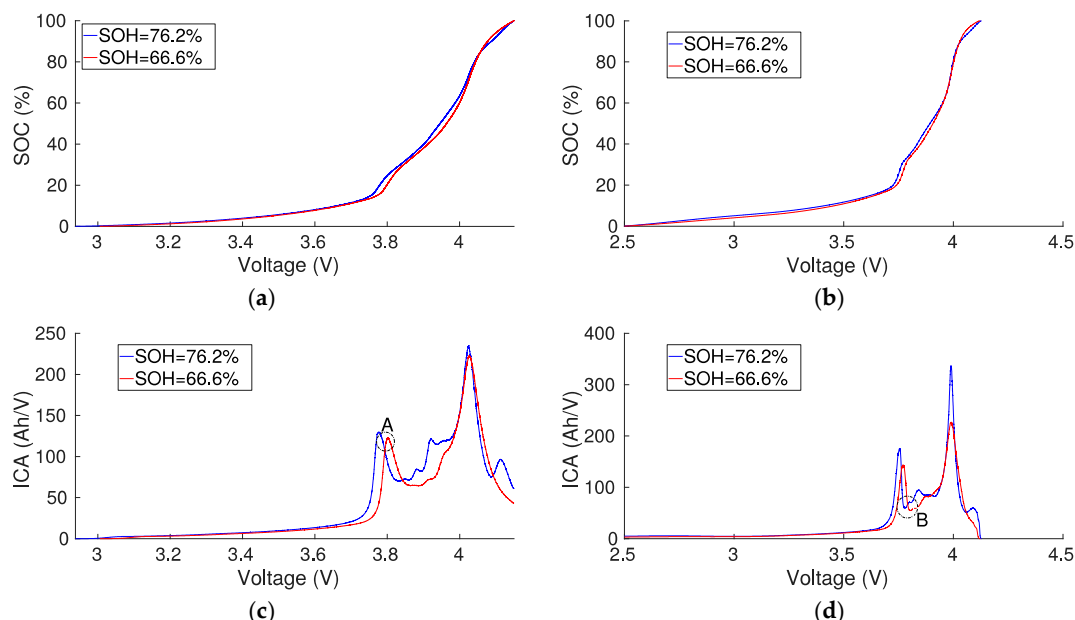


**Figure 7.** Comparison of results for the best sample (SOH = 76.2%) and the worst sample (SOH = 66.6%). (a) OCV charge C/20; (b) OCV discharge C/20; (c) ICA charge C/20; and (d) ICA discharge C/20.

Therefore, the initial step is to identify the rightful indicator for the given chemistry. C/20 charges and discharges have been realized using the 48 half modules. This low rate is synonymous of a quasi-thermodynamic equilibrium and gives a clear vision of the phenomena occurring inside the battery especially the transition phases. Then, an ICA curve comparison from different cells (Figure 7c,d) gives an overview of the changes in peaks and valleys. That observation allows the determination of the aging mechanisms occurring in the studied technology. Of course, these kinds of experiments are very slow and the final target is to be able to increase the charge or discharge rate to its maximum so as to accelerate the measurement protocol.

Most of the time, the raw experimental signal is not directly exploitable. Indeed, in ICA Equation (4), if  $\Delta V = 0$ ,  $ICA \rightarrow \infty$  moreover additive noises are very symptomatic and have to be filtered. Riviere et al. [19] used in their study a numerical Butterworth filter but Li et al. [21] recently highlighted the performance of a moving average filter (MA) represented by Equation (5):

$$y(i) = \sum_{j=1}^M MA(j) \cdot x(i+j-1) \quad \text{with } MA(j) = \frac{1}{M} \quad (5)$$

combined with a Gaussian filter ( $G$ ) in Equation (6):

$$z(i) = \sum_{j=1}^M G(j) \cdot y(i+j-1) \quad \text{with } G(j) = \frac{1}{\sigma\sqrt{2\pi}} \exp - \left( \frac{(j-\mu)^2}{2\sigma^2} \right) \quad (6)$$

In Equations (5) and (6),  $M$  is the number of points considered in the “average window”,  $x$  is the input signal  $y$  an intermediary signal and  $z$  the output signal,  $\mu$  is the mean value of the considered data and  $\sigma$ , called the standard deviation, is a parameter which controls the bandwidth of the filter.

This last technique allows more parametric choices for more flexibility of the experimental datasetting system rather than for example a typical Butterworth filter. Indeed, using Butterworth filter, the time step through the all experimentation has to be the same even during rest times leading sometimes to a useless increase of the dataset. Therefore, the combination of the moving average and the Gaussian filter has been chosen for its flexibility and its simplicity in the coming analysis.

As a result, the voltage variation of peak A and valley B, respectively during C/20 charge and discharge (Figure 7c,d), are linearly proportional to the battery aging state as shown in Figure 8a,b. The quality of the correlation is identified using the least square method.

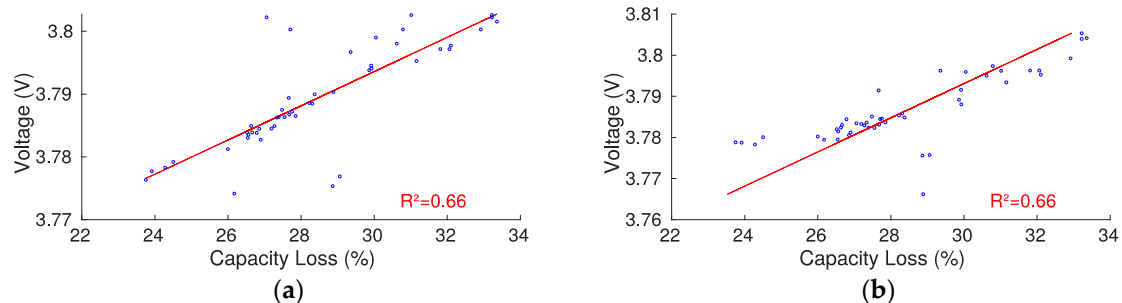


**Figure 8.** (a) Position of peak A variations according the capacity loss; (b) Position of valley B variations according the capacity loss.

A C/20 charge or discharge is a very slow process. In an attempt to reduce and optimize the test time protocol, C/10, C/4, C/3 and C/2 rates were employed and demonstrated that only the peak A, under such charging or discharging constraints, could provide sufficient information about the capacity fading as shown in Figure 9. It should be noted that a peak area analysis was also realized but did not provide any satisfying results.

A C-rate close to the nominal 1C leads to an important distortion of the ICA profile and by consequence to a significant loss of information. For the aforesaid AESC cells, a C/3 charge may afford sufficient information for an estimation of the capacity loss within an optimized processing time.

Even with a C/3 charge rate, the process is still very long. The peak A occurs around 20% of SOC. To save some time, an ICA on a partial charge from 0% up to 30 % of SOC could be considered in our study, instead of using the whole SOC range.

To conclude, this technique could provide an estimation of the SOH for the second life lithium-ion batteries. But the accuracy is directly linked to the C-rate used during the test. The lower is the C-rate

the better will be the estimation. Then, a compromise between the experimental time and the desired accuracy will be necessary.

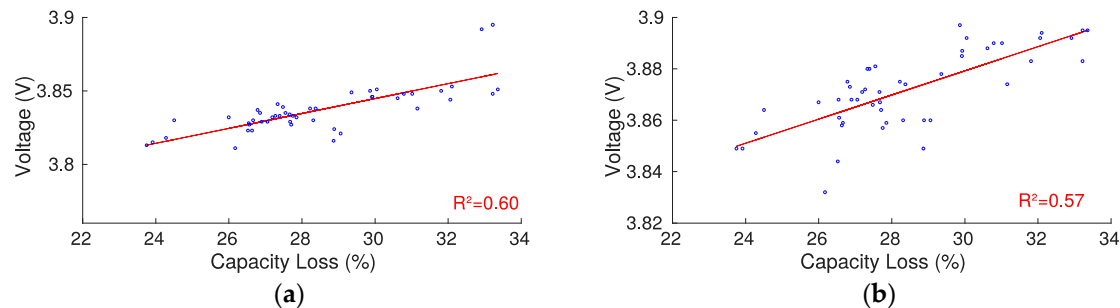


**Figure 9.** Position of peak A variations analysis during charge, (a) C/3, and (b) C/2.

### 2.3.3. Partial Coulometric Counter

The (full) coulometric counter is a straightforward tool used for SOC determination but in some cases it can be employed as a SOH estimation method like by Kong Sooun et al. [26]. Most of the time, this technique requires a complete charge or discharge cycle operated between  $V_{\max,op}$  and  $V_{\min,op}$  as defined in Table 1, leading unfortunately to an important test time.

SOH estimation using coulometric counter through the traditional technique is commonly calculated with the following Equations (7) (for discharge) and (8) (for charge):

$$SOH(Q)[\%] = 100 \frac{Q_{\text{discharged}} V_{\min,op} V_{\max,op}}{Q_{\text{nominal during discharged}}} \quad (7)$$

or

$$SOH(Q)[\%] = 100 \frac{Q_{\text{charged}} V_{\min,op} V_{\max,op}}{Q_{\text{nominal during charged}}} \quad (8)$$

$Q_{\text{discharged}} V_{\min,op} V_{\max,op}$  and  $Q_{\text{charged}} V_{\min,op} V_{\max,op}$  are, respectively, the discharge capacity and charge capacity between  $V_{\min,op}$  and  $V_{\max,op}$ .

We propose to adapt the previous methodology to a partial charge or discharge in order to reduce the test time. After different attempts, the charging phase seems to be the best way to apply directly the partial coulometric counter and can be expressed by Equation (9):

$$SOH(Q)[\%] = 100 \frac{Q_{\text{charged}} V_{\text{pulse-start}} V_{\text{pulse-stop}}}{Q_{\text{nominal charged}} V_{\text{pulse-start}} V_{\text{pulse-stop}}} \quad (9)$$

where  $Q_{\text{charged}} V_{\text{pulse-start}} V_{\text{pulse-stop}}$  is the charge capacity between  $V_{\text{pulse-start}}$  and  $V_{\text{pulse-stop}}$ .  $V_{\text{pulse-start}}$  and  $V_{\text{pulse-stop}}$  have to be optimized in order to achieve the best compromise between the operating time and the sensitivity of the estimator. These voltages are defined under operation and include the influence of the current.

Since a partial charge is going to be used in the following protocol, caution about the starting voltage and the length of the experiment has to be taken into account. In fact, Figure 10 highlights that the transient behaviour of a charge pulse is not the same and mainly depends on the initial voltage level of the half module. To reach the charge profile of the reference curve, few seconds are necessary for a pulse at an initial low voltage (like Pulse 1 in Figure 10) while a 400-second interval is mandatory for a pulse at an initial high voltage (like Pulse 2 in Figure 10). This transient phase is consistent with the transition from the OCV curve—when the battery was at rest—to the 1C charge curve. The characteristics of this transient response depend on the battery impedance which is itself SOC dependent. We noted from other tests that the C-rate can also influence the shape of the transient.

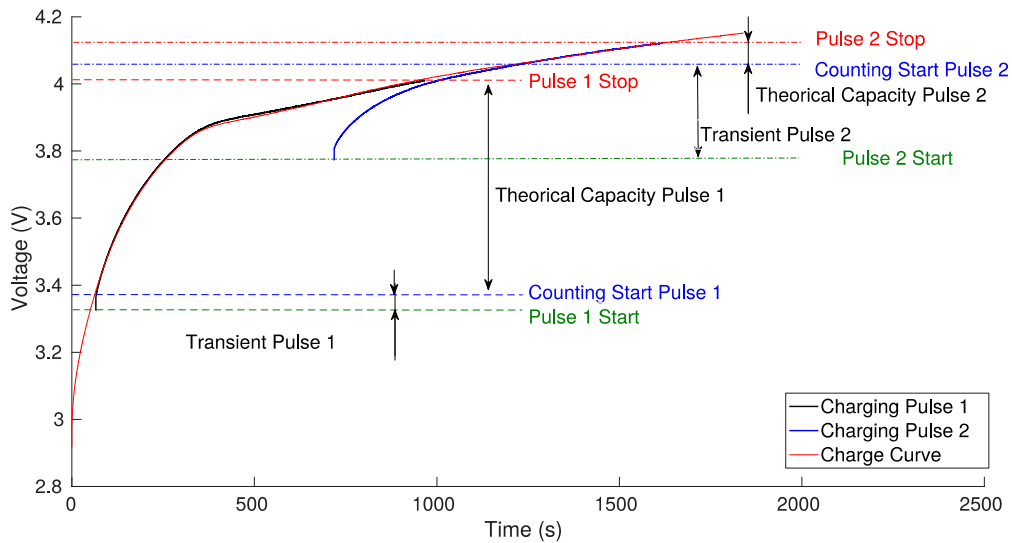


**Figure 10.** Voltage transient phenomenon according to the initial voltage level of a charge pulse 1C/CC.

According to the previous observation, the transient behaviour has to be taken into account for an accurate capacity measurement. Therefore, the capacity counting has to be delayed from the starting point of the pulse, as shown in Figure 11.

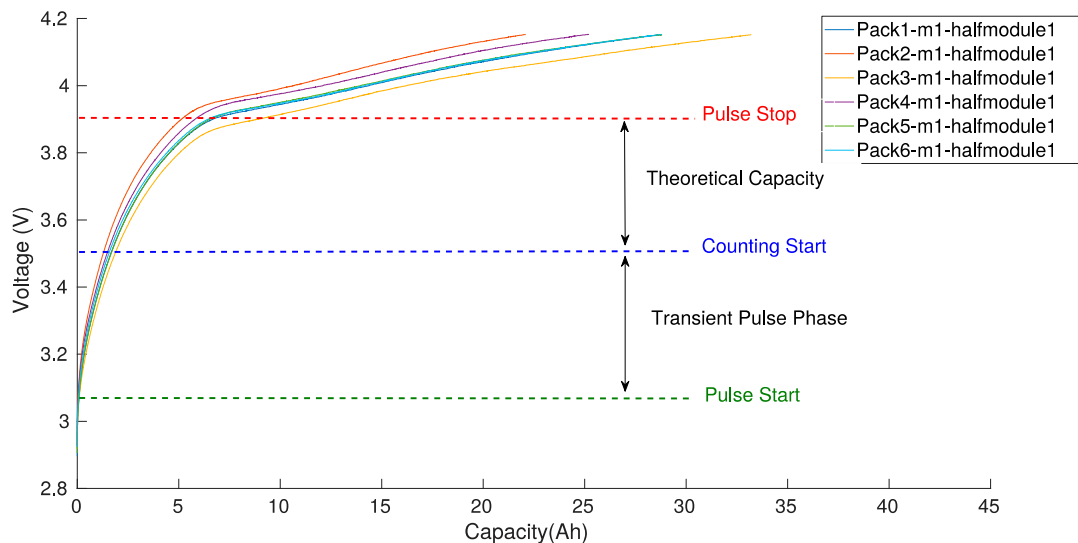


**Figure 11.** Example of pulse start, counting start and pulse stop limits represented on the reference curves.

Taking into account the previous observations, experimental results based on the second life battery test campaign are illustrated by Figure 12. The partial capacity of each cell is measured between two voltage thresholds (3.4 V and 3.8 V) that could correspond to a charge pulse of 300 s at 1C/CC with a counting start occurring 100 s after the beginning. Initially, the cell is considered as fully discharged. The quality of the correlation between the partial capacity and the capacity loss is identified using the least square method.

The  $R^2$  coefficient value ( $R^2 = 0.69$ ) of the correlation highlights a good trend between the partial capacity charged and the capacity loss. The rapidity of the test and its easy implementation should make this methodology a real asset for offline SOH estimations.

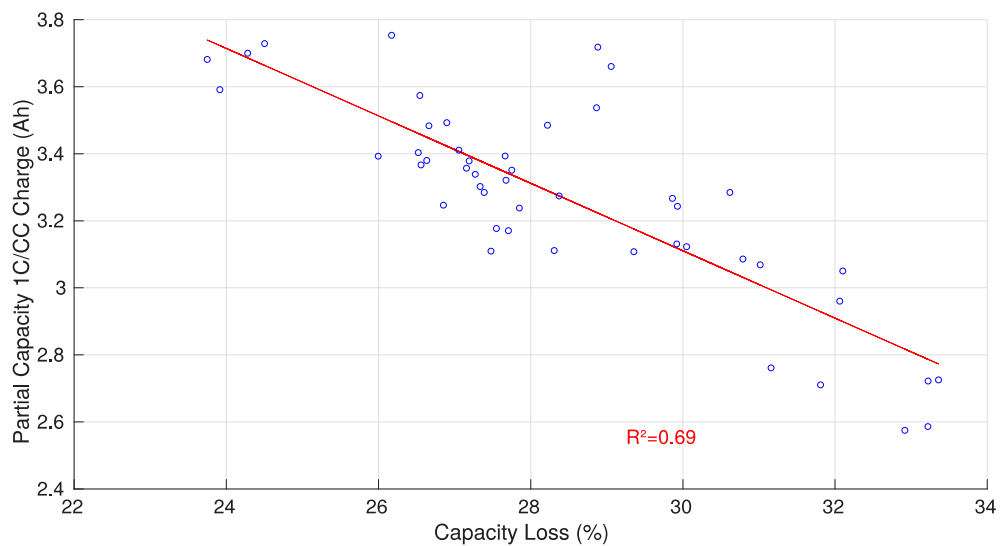


**Figure 12.** Evolution of the partial capacity charged between two voltage levels according the capacity loss.

### 3. Comparison between Methods for Fast Characterization of SOH

According to the foregoing section, the partial coulometric counter appears to be the most accurate method for a SOH estimation. Methods were previously based on a systematic measurement of all the modules under test. In order to shorten the duration of the SOH estimation campaign, we propose a protocol based on the full measurement of only 6 modules, considered as reference and a partial measurement of the others. Each of the 6 modules was selected randomly from six different vehicles. More “reference” modules could be used but it would lead to an increase of prerequisite data and test time. In the following analysis, the three SOH determination methods have been compared using the 6 same references. The quality of the correlation is again identified using the least square method.

#### 3.1. CV Charge Phase Capacity Estimation Method

Through measurements during the CV charge phase according to Section 2.3.1,  $B$  coefficients for the six reference cells are determined and represented according to the total capacity of each cell in Figure 13.

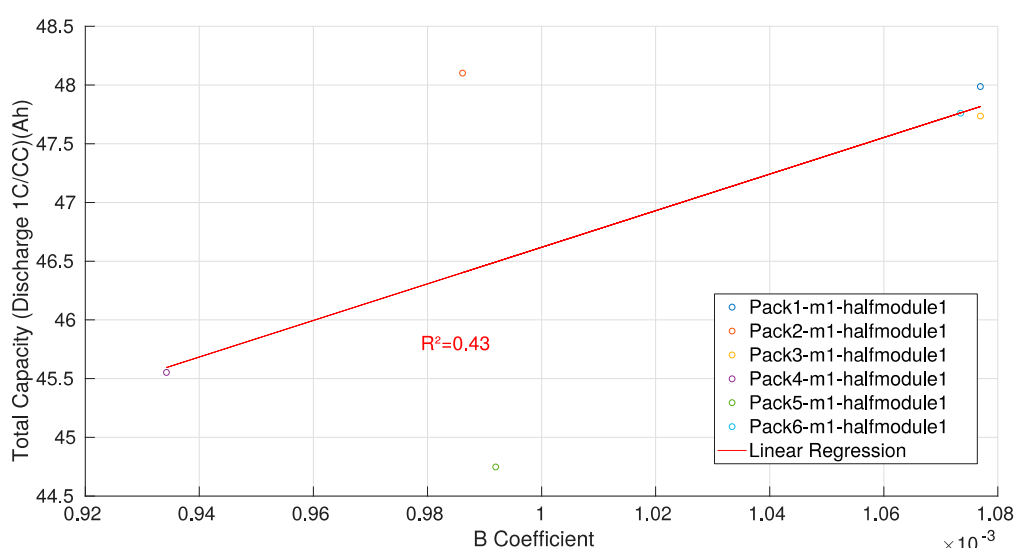


**Figure 13.** Linear relation between measured capacity and  $B$  coefficient for the six references.

From Figure 13, we can deduce in this specific case Equation (10):

$$\text{TotalCapacity(Ah)} = 15577 \times B + 31.042 \quad (10)$$

Then, from the experimental determination of the  $B$  coefficient of the different tested batteries, we can calculate with Equation (10), an estimation of the capacity illustrated in Figure 14. This representation includes 42 half modules (among the 48 half modules, six have been taken as reference). The average absolute error of the estimation is equal to 2.5% with a maximum of 5.7%.

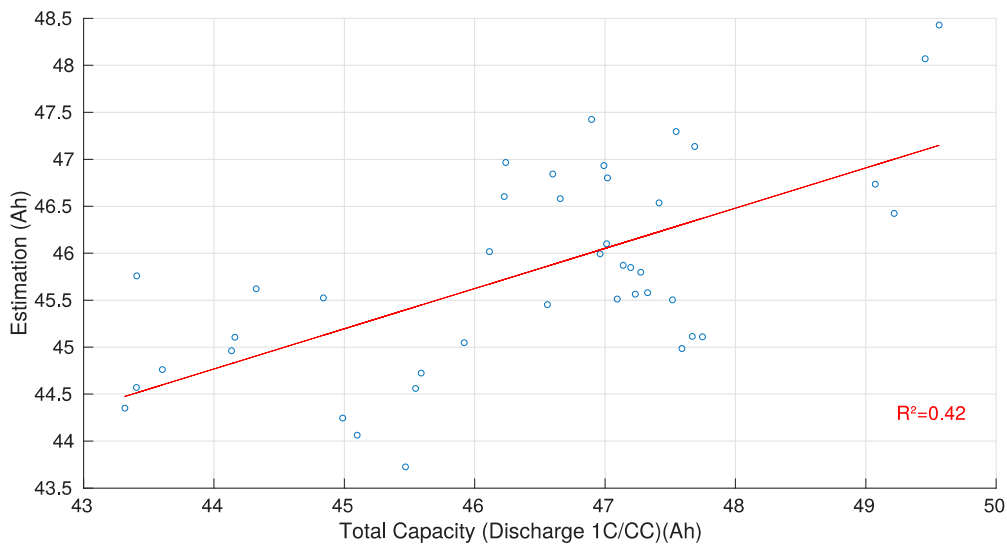


**Figure 14.** Capacity measurement compared with the capacity estimated from the CV phase technique.

### 3.2. ICA Capacity Estimation Methodology

Through the ICA analysis according to Section 2.3.2, peak A voltage position for the six reference cells, under a charge with a C/3 rate, is determined and represented according to the total capacity of each cell in Figure 15.

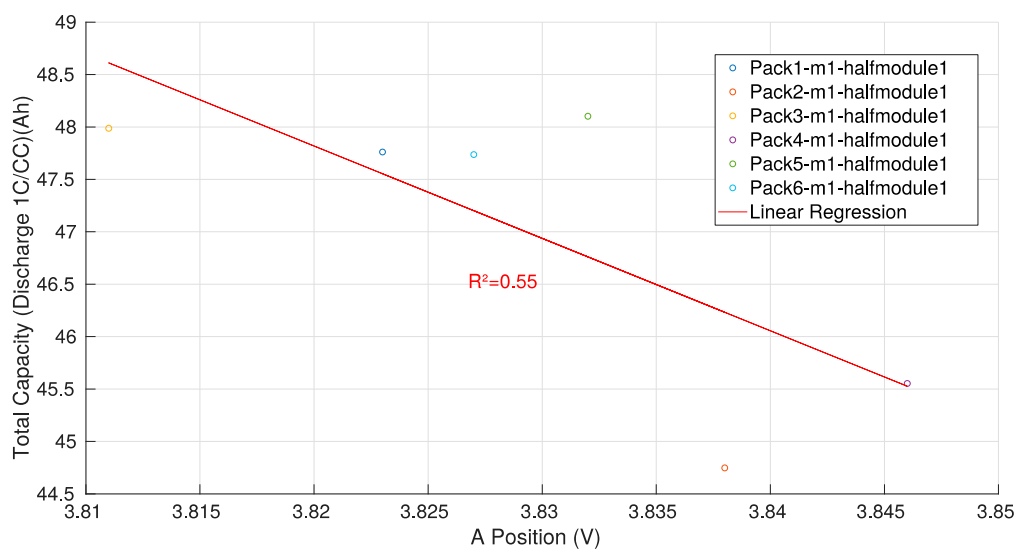


**Figure 15.** Relation between measured capacity and peak A position for the six references.

From Figure 15, we can deduce in this specific case Equation (11):

$$\text{TotalCapacity(Ah)} = -88.098 \times \text{PeakAVoltage(V)} + 384.35 \quad (11)$$

Then, from the experimental determination of the Peak A voltage position of the different tested batteries, we can calculate with Equation (10), an estimation of the capacity illustrated in Figure 16. This representation includes 42 half modules (among the 48 half modules, six have been taken as reference). The average absolute error of the estimation is equal to 1.8% with a maximum of 5.1%.

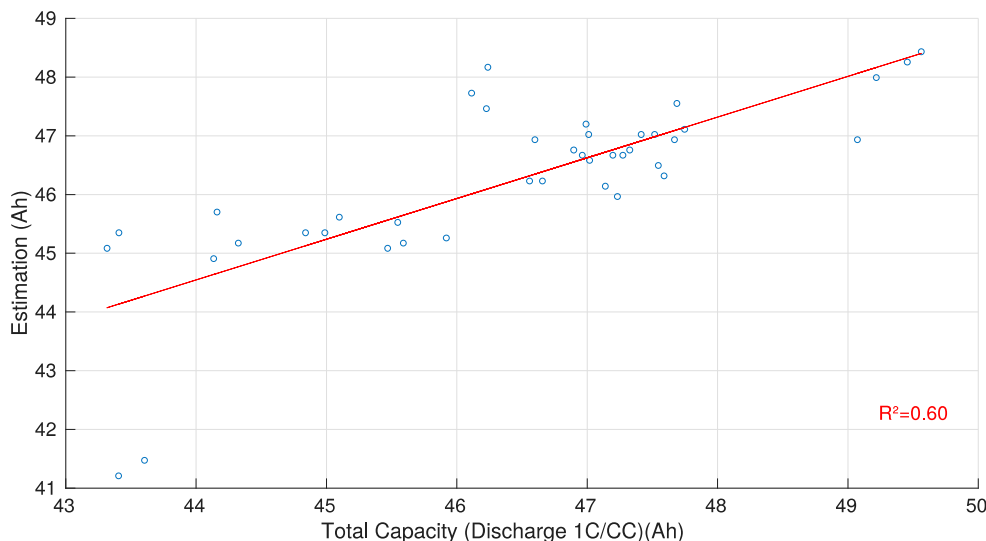


**Figure 16.** Capacity measurement compared with the capacity estimated from the ICA technique.

### 3.3. Partial Coulometric Counter

Through the measurement of the partial coulometric counter according to Section 2.3.3, partial capacities for the six reference cells are determined during a charge cycle and linked to the total capacity of each cell in Figure 17.

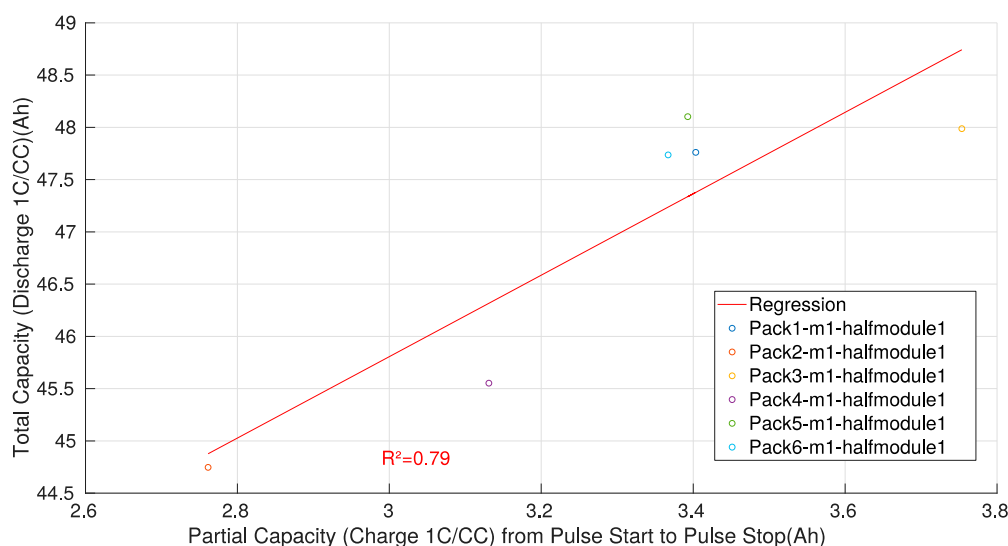


**Figure 17.** Capacity estimation using the regression curve based on the 6 references.

The linear relation in the case of this study can be modelled by Equation (12):

$$\text{TotalCapacity(Ah)} = 3.8967 \times \partial\text{CapacityMeasured(Ah)} + 34.1164 \quad (12)$$

As a result, Figure 18 shows the correlation between the nominal capacity measured during a full CC discharge 1C and the estimated capacity of the partial coulometric counter. The representation includes 42 half modules (among the 48 half modules, six have been taken as reference). The quality of the correlation is identified using the least square method ( $R^2 = 0.69$ ). The average absolute error of the estimation is equal to 1.6% with a maximum of 5.1%.

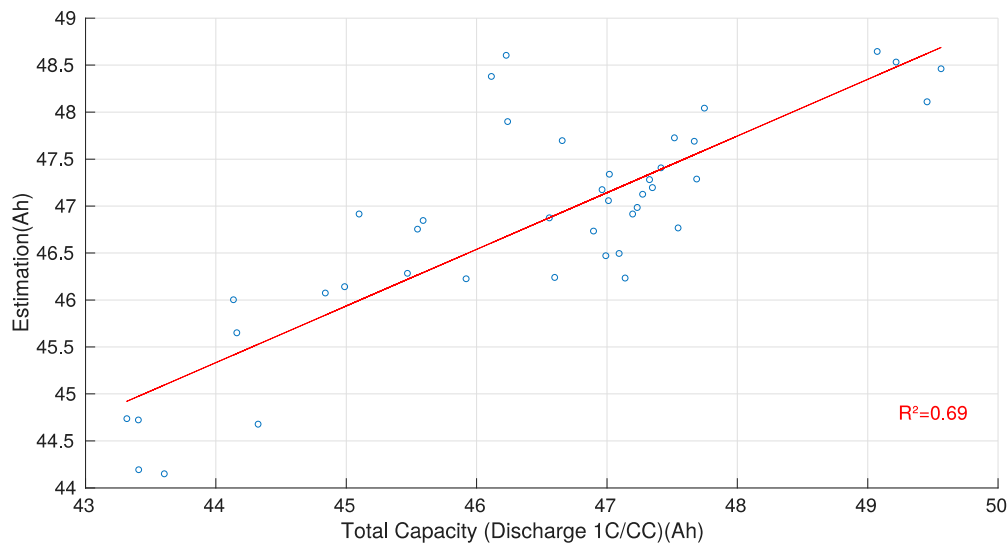


**Figure 18.** Capacity measurement compared with the capacity estimated from the coulometric counter technique.

### 3.4. Synthesis

The following Table 2 represents a synthesis of the different estimation methodologies.

**Table 2.** Comparison of the SOH methodologies applied to second life batteries.

Method	$R^2$	Average Absolute Error	Maximum Absolute Error	Estimated Test Time (s)	Pack Estimation Suitability
Phase CV	0.42	2.5	5.7	1050	-
ICA	0.60	1.8	5.1	3240	++
Partial counter	0.69	1.6	5.1	300	+

In Table 2, the estimated test time considers that the measurement is realized with a battery initially discharged both for the ICA and the partial counter techniques and partially charged (CC phase charge already realized) for the phase CV protocol. The practical duration would include the discharge/charge and rest phases which last approximately up to 90 min.

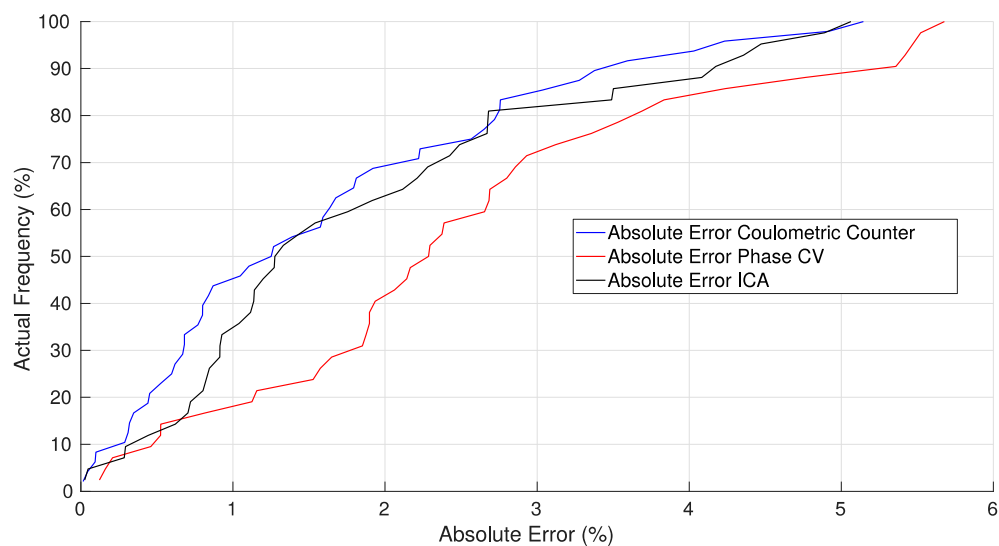
Simultaneity of the measurements could be time saving and protocols applicable directly to a pack should be promoted as much as possible. Therefore, the column pack estimation suitability indicates if the technique is compatible with a direct measurement on the battery pack.

Figure 19 highlights the cumulative distributions of the absolute error related to the different estimation methodologies. From this representation, one can see that if 90% of the modules are considered, the maximum error is lower for the coulometric counter than for the other methods. The phase CV technique has the worst accuracy. In addition, if we only focus on the  $R^2$  of the

different methodologies represented in Table 2, we can again eliminate the CV phase technique in such offline measurements.

From the previous comparison, we can also conclude that the coulometric counter offers the best accuracy regarding the average and the maximum absolute error.

It should be noted that the result of the ICA technique is quite similar. The difference between these two methodologies is the test time that is shorter for the coulometric counter taking into account that the estimation is performed module by module.



**Figure 19.** Cumulative distribution of the absolute error for the different estimations.

If the test of a full pack is considered, the performances of the previous methods change. Indeed, during the full discharge of a pack, the first cell reaching the low voltage limit will trigger the security of the BMS, leading naturally to the stop of the discharge protocol. By consequence, all the modules will not have the same voltage and some of them will not be totally discharged. The partial coulometric counter methodology was applied on cells with a SOC equals to 0% and it is very difficult to estimate without more investigations the impact of a measure starting from another SOC. Regarding the ICA technique, the peak A that gives the information necessary to the capacity estimation is situated around 20 % of SOC. The sensitivity of this methodology to the level of the initial SOC is expected lower than for the coulometric counter. By consequence, the ICA method could be more appropriate for the test of a full pack excluding the measurement of individual modules (based on condition of having sufficient test channels).

#### 4. Conclusions

Three fast characterization methods to determine the full capacity fading of a battery have been tested in this paper. The CV phase protocol proved to be inefficient in the context of real second life lithium-ion batteries. While the ICA technique can only be applied to a whole battery pack mainly for time constraint reason, the generic methodology based on a partial coulometric counter has been proposed and experimentally validated. Each technique has an equivalent accuracy but can only be used on a pack level or on a module level, depending on the methodology chosen. In addition to giving an average absolute error of 1.6% and a maximum error equals to 5.1%, the new protocol has the advantage to determine the capacity fading without any fresh references. Indeed, in this case scenario only six second life reference batteries are necessary to build the needful trend employed to estimate the capacity of the entire experimental campaign.

Literature about second life batteries is quasi nonexistent and comparisons of the results obtained during our experimental campaign with other studies are difficult. Despite that deficiency of information, several interesting points emerged from the previous analysis.

First, through the use of the ICA or the kinetic of the CV phase techniques, it clearly appears that real life aging does not match synthetic aging realized in laboratories, like in [19] or in [22]. Most of the time, cells are placed into a climatic chamber, then a predetermined cycle is chosen and applied for weeks. The atmosphere temperature around the tested cell is raised and precisely controlled in order to accelerate the aging phenomenon in accordance with Arrhenius' law as explained in Redondo-Iglesias et al. [27]. However, in our case, all the batteries originate from different vehicles, by consequence their aging behaviour cannot be the same through time. Indeed, the diversity of the cycle life of the vehicles induces a unique combination of aging mechanisms that leads to a complete heterogeneity of the modules from a vehicle to another. This observation can be extended to the battery pack, where a module could be different from another. This is mainly due to the existence of an unequal temperature gradient inside the casing and sometimes to unequal electrical constraints. These remarks could explain that an aging law which fits correctly for laboratory aging would not be suitable for real-life aging. Barré et al. [28] worked on statistical predictions that take into account future behavior but this approach implies to know all the cycle life of the studied battery.

Future improvements about the optimal counting start identification linked to the transient and the exact time length of the capacity counting have to be studied in order to consolidate the accuracy and the robustness of the proposed new methodology.

Further works would be necessary to complete the characterization method by classification of the second life batteries. This categorization would clearly lean on the measured SOH of the cells but should integrate other criteria. Indeed, the interaction of the multiple aging mechanisms during the first life of identical cells are even more complicated to predict during the second life of cells with different histories. Classification of second life cells could allow to put together cells that aged in a similar way (similar combination of aging mechanisms) and this point would facilitate a better SOH prediction for each group of cells.

**Author Contributions:** H.Q., S.P., P.V., and E.R.-I. conceived and designed the experiments; H.Q. performed the experiments; H.Q., S.P., P.V., and E.R.-I. analysed the data; H.Q. wrote the paper; and S.P., P.V., and E.R.-I. proofread the paper.

**Funding:** This research was funded by National French Association for Technological Research (ANRT) and the company CARWATT.

**Conflicts of Interest:** The authors declare no conflict of interest.

## References

1. International Energy Agency. *Global EV Outlook 2018*; International Energy Agency: Paris, France, 2018. [[CrossRef](#)]
2. The Paris Declaration on Electro-Mobility and Climate Change and Call to Action. Available online: <https://unfccc.int/news/the-paris-declaration-on-electro-mobility-and-climate-change-and-call-to-action> (accessed on 29 November 2019).
3. New Life for Electric Vehicle Batteries—California Energy Storage Showcase. Available online: [https://www.energy.ca.gov/research/energystorage/tour/ev\\_batteries/](https://www.energy.ca.gov/research/energystorage/tour/ev_batteries/) (accessed on 29 November 2019).
4. Electric Vehicle Technology to Power New Nissan Office in Europe. Available online: <https://europe.nissannews.com/en-GB/releases/release-143213-electric-vehicle-technology-to-power-new-nissan-office-in-europe/> (accessed on 29 November 2019).
5. Joint Japan-France Demonstration of Energy Storage System Project Utilization of used Lithium-Ion Batteries from Electric-Powered Vehicles. Available online: [https://www.mitsubishi-motors.com/publish/pressrelease\\_en/corporate/2015/news/detailf710.html](https://www.mitsubishi-motors.com/publish/pressrelease_en/corporate/2015/news/detailf710.html) (accessed on 29 November 2019).
6. Powerwall—The Tesla Home Battery. Available online: <https://www.tesla.com/powerwall> (accessed on 29 November 2019).

7. Eaton—Energy Storage. [En ligne]. Available online: <https://www.eaton.com/gb/en-gb/products/energy-storage.html> (accessed on 29 November 2019).
8. Carwatt. Available online: <http://www.carwatt.net/> (accessed on 29 November 2019).
9. Berecibar, M.; Gandiaga, I.; Villarreal, I.; Omar, N.; Van Mierlo, J.; Van den Bossche, P. Critical review of state of health estimation methods of Li-ion batteries for real applications. *Renew. Sustain. Energy Rev.* **2016**, *56*, 572–587. [[CrossRef](#)]
10. Plett, G.L. Extended Kalman filtering for battery management systems of LiPB-based HEV battery packs. *J. Power Sources* **2004**, *134*, 252–261. [[CrossRef](#)]
11. Remmlinger, J.; Buchholz, M.; Soczka-Guth, T.; Dietmayer, K. On-board state-of-health monitoring of lithium-ion batteries using linear parameter-varying models. *J. Power Sources* **2013**, *239*, 689–695. [[CrossRef](#)]
12. Ragsdale, M.; Brunet, J.; Fahimi, B. A novel battery identification method based on pattern recognition. In Proceedings of the 2008 IEEE Vehicle Power and Propulsion Conference (VPPC), Harbin, China, 3–5 September 2008.
13. Zenati, A.; Desprez, P.; Razik, H.; Rael, S. Impedance measurements combined with the fuzzy logic methodology to assess the SOC and SOH of lithium-ion cells. In Proceedings of the 2010 IEEE Vehicle Power and Propulsion Conference (VPPC), Lille, France, 1–3 September 2010.
14. Cho, S.; Jeong, H.; Han, C.; Jin, S.; Lim, J.H.; Oh, J. On-line monitoring of capacity fade in lithium-ion batteries. *J. Chem. Eng. Jpn.* **2012**, *45*, 983–994. [[CrossRef](#)]
15. Dai, H.; Wei, X.; Sun, Z. A new SOH prediction concept for the power lithium-ion battery used on HEVs. In Proceedings of the 2009 IEEE Vehicle Power and Propulsion Conference (VPPC), Dearborn, MI, USA, 7–10 September 2009.
16. Lu, L.; Han, X.; Li, J.; Hua, J.; Ouyang, M. A review on the key issues for lithium-ion battery management in electric vehicles. *J. Power Sources* **2013**, *226*, 272–288. [[CrossRef](#)]
17. Bloom, I.; Jansen, A.N.; Abraham, D.P.; Knuth, J.; Jones, S.A.; Battaglia, V.S.; Henriksen, G.L. Differential voltage analyses of high-power lithium-ion cells. *J. Power Sources* **2005**, *139*, 295–303. [[CrossRef](#)]
18. Piłatowicz, G.; Marongiu, A.; Drillkens, J.; Sinhuber, P.; Sauer, D.U. A critical overview of definitions and determination techniques of the internal resistance using lithium-ion, lead-acid, nickel metal-hydride batteries and electrochemical double-layer capacitors as examples. *J. Power Sources* **2015**, *296*, 365–376. [[CrossRef](#)]
19. Riviere, E.; Venet, P.; Sari, A.; Meniere, F.; Bultel, Y. LiFePO<sub>4</sub> Battery State of Health Online Estimation Using Electric Vehicle Embedded Incremental Capacity Analysis. In Proceedings of the 2015 IEEE Vehicle Power and Propulsion Conference (VPPC), Montreal, QC, Canada, 19–22 October 2015.
20. Anseán, D.; González, M.; Blanco, C.; Viera, J.C.; Fernández, Y.; García, V.M. Lithium-ion battery degradation indicators via incremental capacity analysis. In Proceedings of the 2017 IEEE International Conference on Environment and Electrical Engineering and 2017 IEEE Industrial and Commercial Power Systems Europe (EEEIC/I&CPS Europe), Milan, Italy, 6–9 June 2017.
21. Li, Y.; Abdel-Monem, M.; Gopalakrishnan, R.; Berecibar, M.; Nanini-Maury, E.; Omar, N.; van den Bossche, P.; Van Mierlo, J. A quick on-line state of health estimation method for Li-ion battery with incremental capacity curves processed by Gaussian filter. *J. Power Sources* **2018**, *373*, 40–53. [[CrossRef](#)]
22. Eddahech, A.; Briat, O.; Vinassa, J.-M. Determination of lithium-ion battery state-of-health based on constant-voltage charge phase. *J. Power Sources* **2014**, *258*, 218–227. [[CrossRef](#)]
23. Yang, J.; Xia, B.; Huang, W.; Fu, Y.; Mi, C. Online state-of-health estimation for lithium-ion batteries using constant-voltage charging current analysis. *Appl. Energy* **2018**, *212*, 1589–1600. [[CrossRef](#)]
24. Redondo-Iglesias, E.; Venet, P.; Pelissier, S. Global Model for Self-Discharge and Capacity Fade in Lithium-Ion Batteries Based on the Generalized Eyring Relationship. *IEEE Trans. Veh. Technol.* **2017**, *67*, 104–113. [[CrossRef](#)]
25. Dubarry, M.; Truchot, C.; Liaw, B.Y. Synthesize battery degradation modes via a diagnostic and prognostic model. *J. Power Sources* **2012**, *219*, 204–216. [[CrossRef](#)]
26. Ng, K.S.; Moo, C.-S.; Chen, Y.-P.; Hsieh, Y.-C. Enhanced coulomb counting method for estimating state-of-charge and state-of-health of lithium-ion batteries. *Appl. Energy* **2009**, *86*, 1506–1511. [[CrossRef](#)]

27. Redondo-Iglesias, E.; Venet, P.; Pelissier, S. Eyring acceleration model for predicting calendar ageing of lithium-ion batteries. *J. Energy Storage* **2017**, *13*, 176–183. [[CrossRef](#)]
28. Barré, A.; Suard, F.; Gérard, M.; Montaru, M.; Riu, D. Statistical analysis for understanding and predicting battery degradations in real-life electric vehicle use. *J. Power Sources* **2014**, *245*, 846–856. [[CrossRef](#)]



© 2019 by the authors. Licensee MDPI, Basel, Switzerland. This article is an open access article distributed under the terms and conditions of the Creative Commons Attribution (CC BY) license (<http://creativecommons.org/licenses/by/4.0/>).